Supplementary Information for

Multidimensional multiplexing geometric phase metaholography

Jinrun Zhang[1,2,3+], Yajuan Dong[1,2,3+], Pan Li[1,2,3], Jinwei Zeng,[1,2,3*] and Jian Wang[1,2,3*]

[1]Wuhan National Laboratory for Optoelectronics and School of Optical and Electronic Information, Huazhong University of Science and Technology, Wuhan, 430074, China
[2]Hubei Optical Fundamental Research Center, Wuhan 430074, China
[3]Optics Valley Laboratory, Wuhan, 430074, China

+ These authors contributed equally to this work.

* Corresponding author: jwang@hust.edu.cn; zengjinwei@hust.edu.cn

1. The principle of the geometric phase

The geometric phase originates from the interaction between the polarized light and the anisotropic element. Here, we define the Jones matrix of the anisotropic element with θ in-plane rotation angle as

$$\mathbf{T}(x,y) = \mathbf{R}(\theta(x,y)) \cdot \mathbf{J} \cdot \mathbf{R}^{-1}(\theta(x,y)) \tag{S1}$$

where $\mathbf{J} = \begin{bmatrix} t_x & 0 \\ 0 & t_y \end{bmatrix}$, $\mathbf{R}(\theta) = \begin{bmatrix} \cos\theta & -\sin\theta \\ \sin\theta & \cos\theta \end{bmatrix}$. Here, $\mathbf{J}$ is the Jones matrix of the anisotropic element in Cartesian coordinates under normal incidence (z-direction) when its optical axis is parallel to the x-axis. t_x and t_y are the field transmissions from x-polarization to x-polarization, y-polarization to y-polarization, respectively. $\mathbf{R}$ is the in-plane rotation matrix and θ indicates the orientation of the anisotropic axis of the element at a given point (x, y).

When left-/right-handed circularly polarized (LCP/RCP) light normally illuminates the anisotropic element with θ in-plane rotation angle, the transmitted light can be expressed as

$$\begin{aligned} \mathbf{E}_{\text{out}}(x,y) &= \mathbf{T}(x,y) \cdot \mathbf{E}_{\text{in}} \\ &= \begin{bmatrix} \cos\theta & -\sin\theta \\ \sin\theta & \cos\theta \end{bmatrix} \cdot \begin{bmatrix} t_x & 0 \\ 0 & t_y \end{bmatrix} \cdot \begin{bmatrix} \cos\theta & \sin\theta \\ -\sin\theta & \cos\theta \end{bmatrix} \cdot \begin{bmatrix} 1 \\ \pm i \end{bmatrix} / \sqrt{2} \\ &= \frac{(t_x + t_y)}{2\sqrt{2}} \begin{bmatrix} 1 \\ \pm i \end{bmatrix} + \frac{(t_x - t_y)}{2\sqrt{2}} e^{\pm i 2\theta(x,y)} \begin{bmatrix} 1 \\ \mp i \end{bmatrix} \end{aligned} \tag{S2}$$

Equation S2 indicates that the transmitted light is composed of the originally polarized component which has the same polarization as the incident light and the orthogonally polarized component which has the orthogonal polarization with the incidence light. Particularly, the orthogonally polarized light gets $\pm 2\theta$ phase modulation, called geometric phase, while the originally polarized component has no additional phase shift. Therefore, we can modulate the phase profile of the orthogonally polarized component of the transmitted light through the space varying optical axis. Moreover, the geometric phase delay is only related to the rotating angle, and is free from the structure parameters and wavelength. Hence, the geometric phase metasurface can tailor the light in broadband with high robustness.

2. Broadband full-modulation of light enabled by parallel tasking geometric-phase metasurfaces

The parallel tasking method utilizes a pure geometric-phase metasurface, enabling full modulation of light (i.e., simultaneously and independently control over amplitude, phase and polarization) by controlling the orientation angle of the geometric-phase element. Its mechanism is elaborated as follows.

The electric field of an arbitrary propagating light beam in a circular polarization (CP) basis can be expressed as

$$\mathbf{E}(x,y) = A_0(x,y)e^{i\varphi_0(x,y)}\begin{bmatrix} |E_l(x,y)|e^{-i\delta_0(x,y)/2} \\ |E_r(x,y)|e^{i\delta_0(x,y)/2} \end{bmatrix} \tag{S3}$$

Here, $A_0(x,y)$, $\varphi_0(x,y)$, $E_l(x,y)$, $E_r(x,y)$, $\delta_0(x,y)$ are the amplitude profile, phase profile, normalized amplitude profile of the LCP component, normalized amplitude profile of the RCP component, and relative phase difference profile between LCP and RCP components of the generated beam, respectively. Assuming the incident beam has CP, in order to modulate the incident beam into an arbitrary beam, we divide the orientation angle of a geometric-phase element (unitcell) into 3 sub-angles: $\theta_\varphi, \theta_i, \theta_s$ for phase, amplitude and polarization modulation, respectively, as shown in Fig. S1.

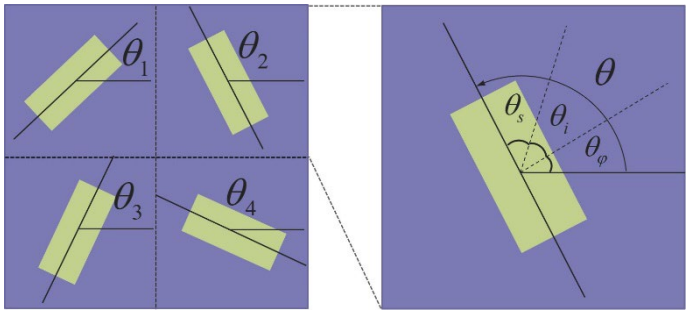

Fig. S1. Schematic diagram of the parallel tasking method.

First, we use θ_φ to modulate the phase profile of the light. Based on the geometric-phase principle, the transmitted beam will get $\varphi = \pm 2\theta_\varphi$ phase delay, while the sign is dependent on the handedness of the transmitted orthogonal CP component. Particularly, $\theta_{1\varphi}$ and $\theta_{2\varphi}$ are used to modulate the phase profile of RCP component of the transmitted light as $\varphi_1 = 2\theta_{1\varphi} = \varphi_2 = 2\theta_{2\varphi} = \varphi_0(x,y) + \delta_0(x,y)/2$; while, $\theta_{3\varphi}$ and $\theta_{4\varphi}$ are used to modulate the phase profile of LCP component of the transmitted light as $\varphi_3 = -2\theta_{3\varphi} = \varphi_4 = -2\theta_{4\varphi} = \varphi_0(x,y) - \delta_0(x,y)/2$.

Second, we use θ_i to modulate the amplitude profile of the light. We introduce the opposite sub-angle to the adjacent unitcells ($\theta_{1i} = -\theta_{2i}, \theta_{3i} = -\theta_{4i}$) in a row, and it will

result in a phase difference between them. Here, we consider that the transmitted beams from two adjacent unitcells overlap with each other owing to the subwavelength period. Therefore, the amplitude of the final interference beam for the RCP component has the expression of $A_0(x,y)\left|E_r(x,y)\right| = \cos(\theta_{1\mathrm{i}} - \theta_{2\mathrm{i}}) = \cos 2\theta_{1\mathrm{i}}$. Similarly, the interference beam for the LCP component is $A_0(x,y)\left|E_l(x,y)\right| = \cos(\theta_{3\mathrm{i}} - \theta_{4\mathrm{i}}) = \cos 2\theta_{3\mathrm{i}}$.

Third, we use θ_s to modulate the polarization profile of the light. The θ_s introduces an opposite phase gradient ($\pm 2k \cdot x$, k is the phase gradient, x is the column number of the metasurface) to the odd and even rows of the metasurface. Therefore, when incident LP light illuminates the metasurface, the odd and even rows of the metasurface will diffract the RCP and LCP components of the transmitted beam at the same diffraction angle, respectively. Similarly, the diffracted LCP and RCP beams from the odd and even rows, respectively, can be considered as one overlapped beam because of the subwavelength period. Combined with phase and amplitude modulation induced by θ_φ and θ_i in the odd and even rows, they can achieve independent and complete polarization modulation. Therefore, $2\theta_{1s} = -2\theta_{3s} = 2kx$. Meanwhile, the encoding process of the three stages is shown in Fig. S2.

Based on the independent phase modulation controlled by the sub-angles of θ_φ, θ_i, θ_s, the metasurface can eventually enable full modulation of light. The relationship between the transmitted light and the rotating angle of the unitcells can be expressed as:

$$\begin{aligned}
\theta_1 &= \theta_{1\varphi} + \theta_{1i} + \theta_{1s} = \frac{\varphi_0(x,y) + \delta_0(x,y)/2 + \arccos[A_0(x,y)\left|E_r(x,y)\right|]}{2} + kx \\
\theta_2 &= \theta_{2\varphi} + \theta_{2i} + \theta_{2s} = \frac{\varphi_0(x,y) + \delta_0(x,y)/2 - \arccos[A_0(x,y)\left|E_r(x,y)\right|]}{2} + kx \\
\theta_3 &= \theta_{3\varphi} + \theta_{3i} + \theta_{3s} = -\frac{\varphi_0(x,y) - \delta_0(x,y)/2 - \arccos[A_0(x,y)\left|E_l(x,y)\right|]}{2} - kx \\
\theta_4 &= \theta_{4\varphi} + \theta_{4i} + \theta_{4s} = -\frac{\varphi_0(x,y) - \delta_0(x,y)/2 + \arccos[A_0(x,y)\left|E_l(x,y)\right|]}{2} - kx
\end{aligned} \tag{S4}$$

Further, we can also express it as

$$
\begin{aligned}
&A(x,y)=\sqrt{\cos^2\left[2\theta_{1i}(x,y)\right]+\cos^2\left[2\theta_{3i}(x,y)\right]}\\
&\varphi(x,y)=\theta_{1\varphi}(x,y)-\theta_{3\varphi}(x,y)\\
&\left|E_l(x,y)\right|=\frac{\cos\left[2\theta_{3i}(x,y)\right]}{\sqrt{\cos^2\left[2\theta_{1i}(x,y)\right]+\cos^2\left[2\theta_{3i}(x,y)\right]}}\\
&\left|E_r(x,y)\right|=\frac{\cos\left[2\theta_{1i}(x,y)\right]}{\sqrt{\cos^2\left[2\theta_{1i}(x,y)\right]+\cos^2\left[2\theta_{3i}(x,y)\right]}}\\
&\delta_0(x,y)=2\theta_{1\varphi}(x,y)+2\theta_{3\varphi}(x,y)
\end{aligned}
\tag{S5}
$$

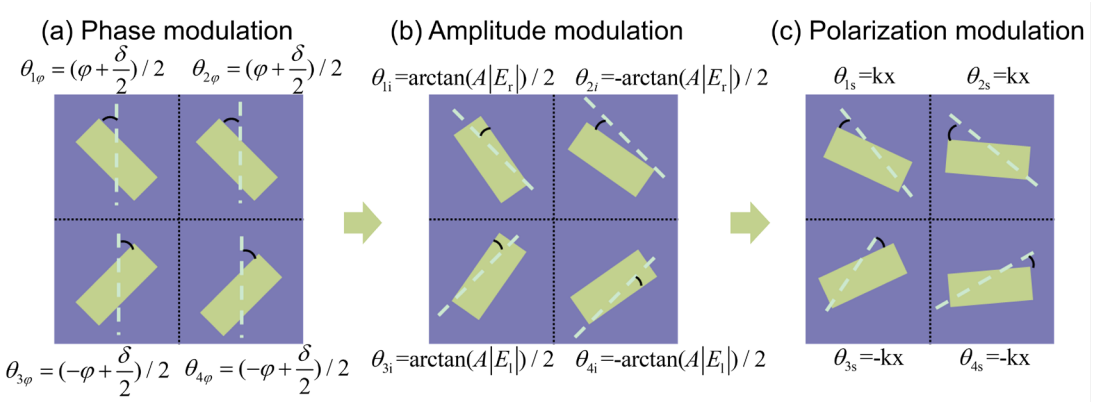

Fig. S2. Flowchart of the phase encoding process in the metasurface.

3. Electric field distribution of the multi-dimensional multiplexing meta-hologram

The electric profile $\vec{\mathbf{E}}_{\text{meta}}^{\text{mul}}$ of the multiplexing hologram is the superposition of multiple channels, which can be expressed as Equation S6. This metasurface has multiplexed holographic images of the letters "A, B, H, U, S, T" as shown in the main manuscript. The exact essential parameters of the metasurface, including the amplitude, phase, and normalized amplitude profile of x-pol. component, normalized amplitude profile of y-pol. component, and relative phase difference profile between x-pol. and y-pol. components are shown in Fig. S2.

$$
\begin{aligned}
\vec{\mathbf{E}}_{\text{meta}}^{\text{mul}} &= \sum_{j=1:N} E_j\cdot\hat{\mathbf{p}}_j\cdot e^{i\vec{\mathbf{k}}_j\cdot\vec{\mathbf{r}}}\\
&= E_A e^{i\vec{\mathbf{k}}_1\cdot x}\begin{bmatrix}1\\ i\end{bmatrix}/\sqrt{2}+E_B e^{i\vec{\mathbf{k}}_1\cdot x}\begin{bmatrix}1\\ -i\end{bmatrix}/\sqrt{2}+E_H e^{i\vec{\mathbf{k}}_2\cdot y}\begin{bmatrix}1\\ 0\end{bmatrix}+E_s e^{i\vec{\mathbf{k}}_2\cdot y}\begin{bmatrix}0\\ 1\end{bmatrix}\\
&\quad+E_U e^{i\vec{\mathbf{k}}_3\cdot(x+y)}\begin{bmatrix}1\\ 1\end{bmatrix}/\sqrt{2}+E_T e^{i\vec{\mathbf{k}}_3\cdot(x+y)}\begin{bmatrix}1\\ 1\end{bmatrix}/\sqrt{2}
\end{aligned}
\tag{S6}
$$

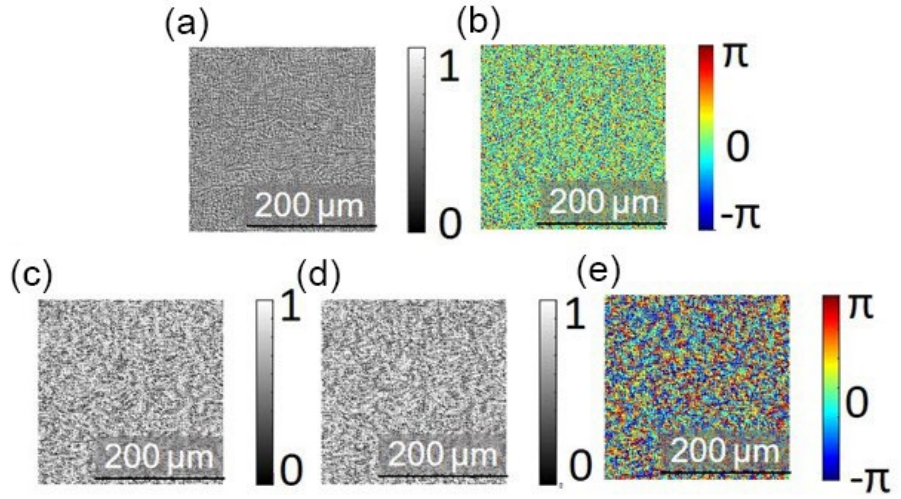

Fig. S2. The electric field profile of the metasurface. (a-e) Amplitude profile, phase profile, normalized amplitude profile of x-pol. component, normalized amplitude profile of y-pol. component, and relative phase difference profile between the x-pol. and y-pol. components of the multiplexing hologram.

4. Fabrication process

We fabricate the metasurface samples by the following process:

(1) SiNx Film Deposition

A 600 nm silicon nitride (SiNx) layer is deposited on the substrate via plasma-enhanced chemical vapor deposition (PECVD) using $SiH_4/NH_3/N_2$ gas mixtures. This step ensures uniform film growth with controlled stress properties, which is critical for minimizing degradation under thermal or mechanical loads.

(2) Cr Hard Mask Preparation

A 50 nm chromium (Cr) layer is deposited by electron beam evaporation. This layer serves two purposes: enhancing conductivity for electron beam lithography (EBL) and acting as a robust hard mask during subsequent etching.

(3) Photoresist Spin-Coating & EBL Patterning

ARP6200.09 photoresist is dynamically dispensed at 500 rpm for initial spreading, followed by high-speed spin-coating at 1500 rpm for 30 seconds. This rotational speed minimizes edge bead effects and improves pattern fidelity across the 389 μm × 389 μm substrate. The metasurface pattern (1024 × 1024 unitcells) is written using a 100 kV electron beam with optimized beam current and alignment.

(4) ICP Etching of Cr and SiNx

Inductively coupled plasma (ICP) etching with Cl_2/Ar gas selectively removes the Cr layer. Subsequently, a CF_4/H_2/Ar gas mixture etches the SiNx layer at 1000 W ICP

power. The H_2 additive enhances sidewall smoothness by passivating reactive dangling bonds.

(5) Cr Removal

Residual Cr is dissolved using a commercial etchant ($Ce(NH_4)_2(NO_3)_6/HNO_3$-based solution) without damaging the SiNx nanostructures.

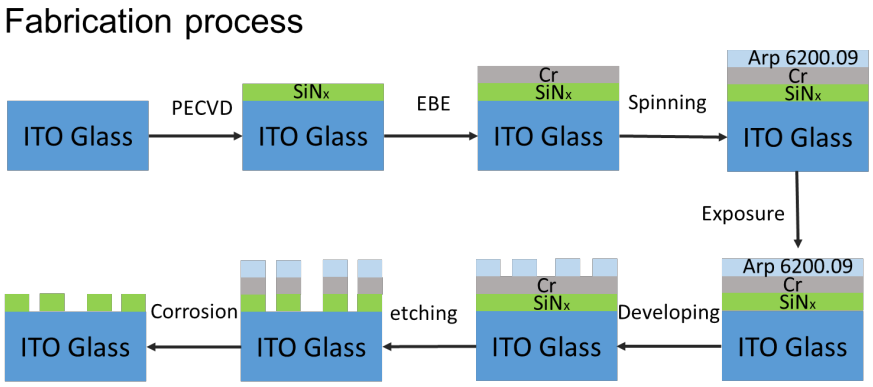

Fig. S3. The fabrication process of the metasurface sample.

5. Optical characterization

To experimentally demonstrate the broadband multi-dimensional multiplexing holography, we use a super-continuum source and an acoustic-optical tunable filter (AOTF) to emit coherent light with different wavelengths. Then, we employ a series of polarization elements including linear polarizers, quarter-wave plates, and half-wave plates to control the polarization of the incident beam. Next, the beam is focused by a lens through the fabricated metasurface sample, and collimated by a lens with the same focal length. Similarly, a series of polarization elements is used to test the polarization of the transmission beam. Finally, we employ a CCD camera to record the holographic image. The general experimental schematics are shown in Fig. S4.

As introduced in the main manuscript, here we illustrate 3 typical scenarios to demonstrate the multi-dimensional multiplexing capability of the proposed metasurface. The specific experimental conditions are elaborated as follows.

A. Fixed input & varied Output (FIVO)

In this scenario, we set the axis of Pol 1 at 0°, so the incident beam is x-polarized light normal to the metasurface, as the fixed input. On the receiving side, we rotate the quarter-wave plate and Pol 2 to distinguish different polarizations of the transmission beams, and the diffraction beams in different directions will be collected by the camera in different positions, as the varied output.

B. Varied Input & fixed output (VIFO)

In this scenario, we set the axis of the Pol 2 as 0° and change the polarization of the incident beam. With the varied input of the holography system, we can observe particular images in the fixed optical channel captured by the camera.

C. Varied Input & varied output (VIVO)

This scenario is the mixture of the previous two cases, while both the input and output have varied conditions. Here we conceal a target information (i.e., the word "HUST") in the holographic images, which can be read with the time-varying polarization and the transverse momentum set for input and output, as shown in the main manuscript.

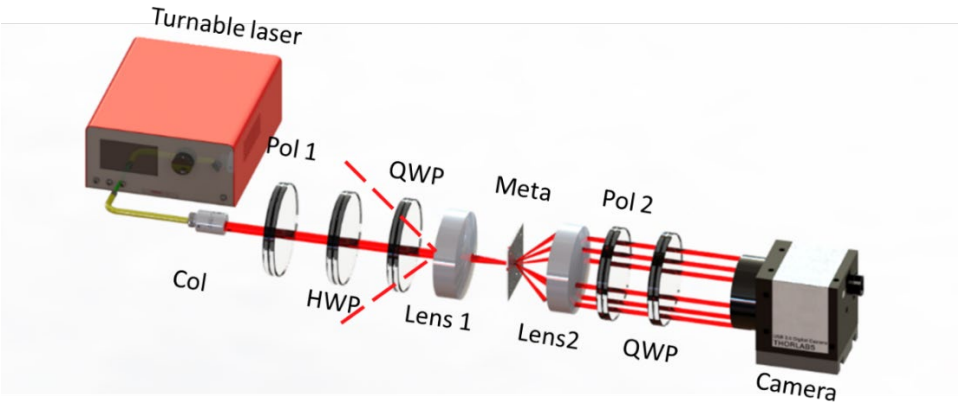

Fig. S4. Experimental setup. Pol: polarizer; HWP: half-wave plate; QWP: quarter-wave plate; Col: collimator; Meta: Metasurface. The red dash lines indicate the possible illumination directions, and the solid red lines after the metasurface indicate the possible transmission directions, as the input and output paths, respectively.

6. Multiplexing of the full-dimensional metasurface based holography multiplexing

In this section, we will discuss the multiplexing hologram based on a full-modulation metasurface and phase-polarization modulation (PP) metasurface. As indicated in the main manuscript, the electric field on the full-modulation metasurface can be expressed as the supposition of each channel:

$$\vec{\mathbf{E}}_{\text{full}}^{\text{mul}} = A(x,y)e^{i\varphi(x,y)}\vec{\mathbf{P}}(x,y) = \sum_{j=1:N} E_{\text{holo}\_j} \cdot \hat{p}_j \cdot e^{i\vec{\mathbf{k}}_j \cdot \vec{\mathbf{r}}} \tag{S7}$$

Here, E_{holo_j} is the electric field of the j-th channel hologram, $\hat{p}_j$ is the polarization of the j-th channel, $\vec{\mathbf{k}}_j$ is the phase gradient of the j-th channel. When x-polarization light illuminates the metasurface, we use optical blocks and polarizers to filter out the undesired channels. The image of the channel-a can be expressed as

$$\vec{\mathbf{E}}_{\text{full}}^{\text{imag}} = \mathrm{F}(E_{\text{holo\_a}}) \cdot \hat{p}_a \tag{S8}$$

Based on the de-multiplexing process, for the ideal full-dimensional meta-hologram, the crosstalk between each channel is minimal. Moreover, the power of the multiplexing field is equally allocated to each channel.

7. Multiplexing of the phase-polarization modulation metasurface based holography multiplexing

The phase-polarization meta-holography lacks amplitude modulation, whose consequence can be elaborated as follows.

To begin with, the phase-polarization meta-holography can have the electric field expressed as

$$\vec{\mathbf{E}}_{\mathbf{PP}}^{\text{mul}} = e^{i\varphi(x,y)}\vec{\mathbf{P}}(x,y) = \exp(\arg(\sum_{j=1:N} E_{\text{holo\_j}} \cdot \hat{p}_j \cdot e^{i\vec{\mathbf{k}}_j \cdot \vec{\mathbf{r}}})) \tag{S9}$$

It loses the amplitude information of the complex multiplexing electric field. Obviously, it cannot be expressed as the exact superposition of the multiplexing channels, and must include an additional noise term

$$\begin{aligned} \vec{\mathbf{E}}_{\text{PP}}^{\text{Mul}} &= \exp(\arg(\sum_{j=1:N} E_{\text{holo\_j}} \cdot \hat{p}_j \cdot e^{i\vec{k}_j \cdot \vec{r}}) \\ &= \sum_{j=1:N} C_j E_{\text{holo\_j}} \cdot \hat{p}_j \cdot e^{i\vec{k}_j \cdot \vec{r}} + \vec{\mathbf{E}}_{\text{noise}} \end{aligned} \tag{S10}$$

The total electric field in the metasurface is composed of non-uniform images in each channel and additional noise. Here C_j is the complex weight for the fields of different channels, $\vec{\mathbf{E}}_{\text{noise}}$ is the noise induced by the phase-polarization based multiplexing. When x-polarized light illuminates the multiplexing hologram, we use the same method to filter out the undesired channels, and the image of the channel-a can be expressed as

$$\begin{aligned} \vec{\mathbf{E}}_{\text{PP}}^{\text{Image}} &= \hat{p}_a \cdot e^{-i\vec{k}_a \cdot \vec{r}} \cdot e^{i\varphi(x,y)}\vec{\mathbf{P}}(x,y) \\ &= C_a E_{\text{holo\_a}} \hat{p}_a + \hat{p}_a \cdot e^{-i\vec{k}_a \cdot \vec{r}} \vec{\mathrm{E}}_{\text{noise}} \end{aligned} \tag{S11}$$

8. Comparison of different multiplexing principles

It is straightforward to understand that perfectly loyal holography is generally impossible without polarization modulation. Therefore, due to the lack of the essential polarization modulation, the phase-only and phase-amplitude modulation metasurfaces cannot produce the exactly accurate holography as the full-modulation

metasurface. As a result, here we mainly compare the multiplexing property between the full-modulation meta-holography and the phase-polarization meta-holography.

Firstly, we compare the energy uniformity (EU) in each channel. We define EU as

$$\mathrm{EU} = \frac{1}{N}\sum_{j=1:N}\left|(P_j - \overline{P})\right| \tag{S12}$$

where P_j is the power of the j-th channel, $\overline{P}$ is the average power of the multiplexing channels. The minimal EU, i.e. all channels share the same energy, indicates an ideal energy allocation of the multiplexing system. For full-modulation metasurface strategy, the energy in each channel can be uniform to reasonably achieve the ideal EU. On the other hand, for phase-polarization metasurfaces, their EU of the multiplexed meta-holograms can be expressed as

$$\mathrm{EU}_{\mathrm{pp}} = \frac{1}{N}\sum_{j=1:N}\left|P_j - \overline{P}\right| = \frac{1}{N}\sum_{j=1:N}\left|C_j \cdot C_j^* - \frac{\sum_{j=1:N} C_j \cdot C_j^*}{N}\right| \tag{S13}$$

We remind that C_j is the complex weight for the fields of different channels, as defined in the multiplexing fields in Equation S10. Without amplitude modulation, such weights are generally not identical to each other, so the phase-polarization metasurface can hardly achieve the ideal EU.

To further investigate the EU, we conduct comprehensive simulations on the energy distribution of multiplexed holograms. As shown in Fig. S5(a) and (b), the multidimensional multiplexed holograms generated by full-modulation metasurfaces and polarization-phase metasurfaces exhibit EU values of 0.0165 and 0.722, respectively. This comparison demonstrates the critical role of amplitude modulation in achieving high-performance multidimensional holography, and also validates the superior capability of full-modulation metasurfaces in handling complex multiplexing requirements.

Secondly, we compare the signal-to-noise ratio (SNR) of multiplexing holographic images based on the different multiplexing methods. Here, we define the noise in the SNR as the excessive noise induced by the multiplexing process at the metasurface projecting on a particular channel (i.e. $Noise_j = \left|(\hat{p}_a \cdot \vec{\mathrm{E}}_{\mathrm{noise}})\right|^2$), which does not include the noise from imperfect fabrication or experimental conditions. Thus, the SNR of phase-polarization metasurface based multiplexing can be expressed as

$$\mathrm{SNR}_j = \frac{P_j}{Noise_j} = \frac{C_j \cdot C_j^*}{\left|(\hat{p}_a \cdot \vec{\mathrm{E}}_{\mathrm{noise}})\right|^2} \tag{S14}$$

Here, with the increase in channel number, the absolute weight of each channel C_j will generally decrease, and thus eventually induce a decrease in SNR. On the other hand, according to Equation 9 in the main manuscript, the full-modulation metasurface does not induce any excessive noise in the multiplexing process, it can achieve an ideal SNR regardless of the number of channels.

Lastly, we provide a direct comparison of the multiplexing performance between the full-dimensional meta-hologram based on a full-modulation metasurface and the phase-polarization meta-hologram based on a phase-polarization metasurface. We use the Fresnel diffraction integral to calculate the holographic images of each polarization at each channel on the image plane of the full-dimensional meta-hologram and phase-polarization meta-hologram. The results shown in Fig. S6 indicate a superior performance of the full-modulation metasurface compared to that of the phase-polarization metasurface.

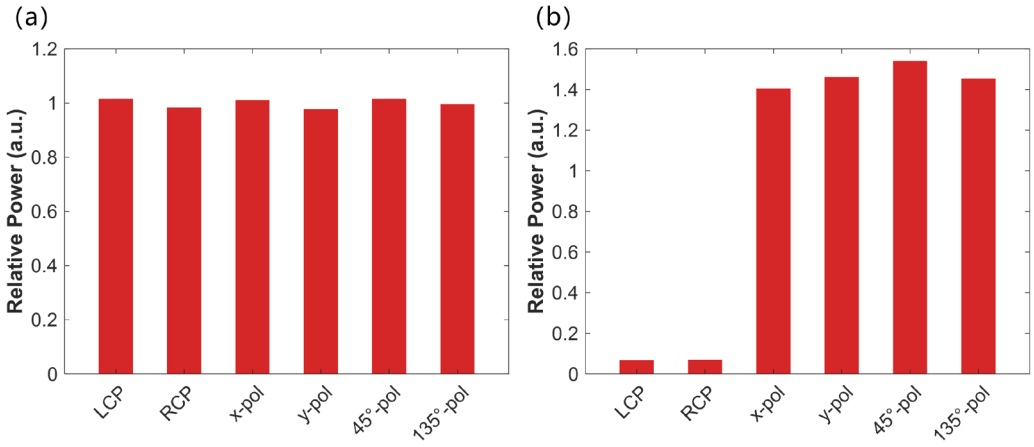

Fig. S5. The simulation energy distribution of the multi-dimensional multiplexing hologram is based on the (a) full-modulation metasurface and (b) phase-polarization modulation metasurface.

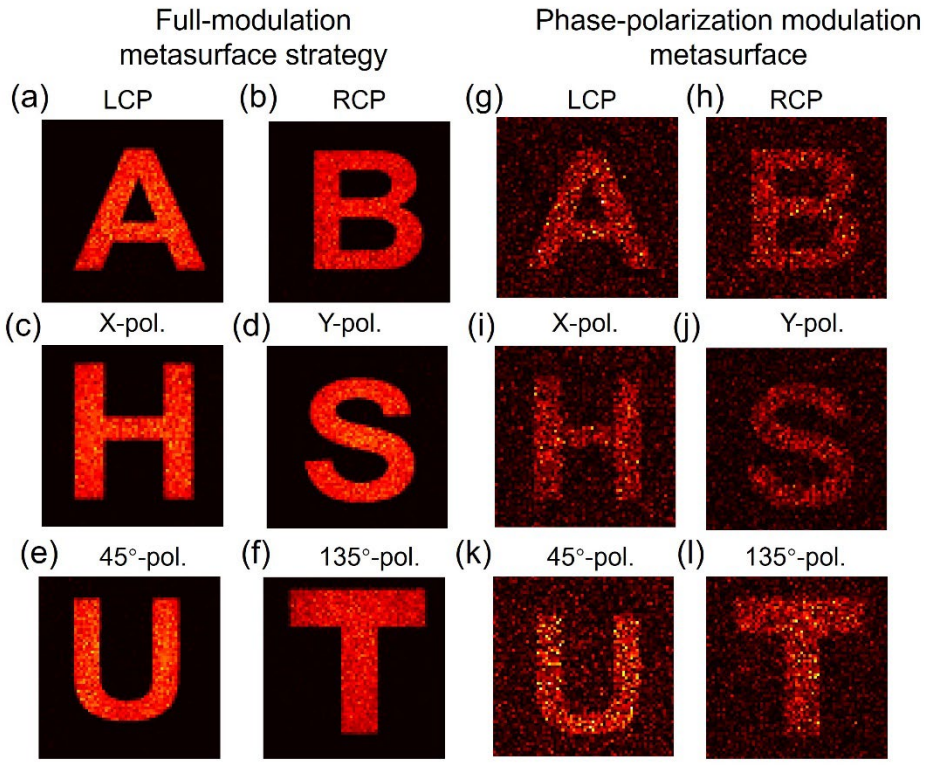

Fig. S6. The simulation results of the multi-dimensional multiplexing hologram based on the (a)-(f) full-modulation metasurface and (g)-(l) phase-polarization modulation metasurface.